



Study on the elastoplastic damage evolution characteristics of suspended cut-off wall of rockfill dam on ultra-deep overburden during construction and long-term operations

Jun Peng^{a,b}, Degao Zou^{a,b}, Yongqian Qu^{a,b,*}, Jingmao Liu^{a,b}, Kai Chen^{a,b}

^a The State Key Laboratory of Coastal and Offshore Engineering, Dalian University of Technology, Dalian, Liaoning 116024, China

^b School of Infrastructure Engineering, Dalian University of Technology, Dalian, Liaoning 116024, China

ARTICLE INFO

Keywords:

Ultra-deep overburden
Suspended cut-off wall
Elastoplastic analysis
Damage cracking
Creep effect

ABSTRACT

Concrete cut-off walls are crucial anti-seepage structures for rockfill dams on overburden. Currently, linear-nonlinear elastic analyses are predominantly used for anti-seepage structures and rockfill, which however cannot accurately describe the real behaviour of cut-off walls. Therefore, an integrated elastoplastic failure analysis method was proposed in which a unified elastic-plastic-creep model for dam and overburden, and plastic damage model and cohesive zone model are combined to separately describe the compressive damage and tensile cracking of concrete cut-off walls. The results indicate that the suspended cut-off wall experiences compressive damage from the bottom upwards on both banks due to high compressive stresses acting nearly perpendicular to the slopes. In-plane bending induces high tensile stresses, leading to vertical cracks and triangular cracking zones on both sides of the wall. Considering long-term creep effects, the damage mode remains largely unchanged, but the damage area and the cracking width increases. This paper elucidates the deformation modes and failure mechanisms, identifies the weak areas, and quantifies the damage of the cut-off wall under construction and long-term operation conditions. This paper provides essential theoretical and technical support for the safety evaluation and design optimisation of cut-off walls of rockfill dams on ultra-deep overburden.

1. Introduction

Overburden foundations are commonly constructed in major river basins worldwide. The Quaternary alluvial sediments in these foundations often extend to depths of several hundred metres and exhibit poor and complex geological conditions. With the continuous development of water energy resources, good dam sites are becoming increasingly scarce, making the construction of deep overburden dams inevitable [1–3]. Rockfill dams are the preferred type of dam to construct on overburden foundations due to their simple construction and strong foundation adaptability. To date, the most popular technique for constructing the foundation of rockfill dams over the overburden and ensuring antiseepage ability is the use of vertical cut-off walls [4], with representative projects such as the Venango project (Italy) completed in 1956 [5], the Manicouagan 3 project (Canada) with a cut-off wall depth of 131 m [6], the Yele project (China) with an overburden thickness of 400 m [7], and the Changhe Dam project (China) with a height of 240 m

[8]. However, once problems occur with the cut-off wall of deep soil, such as compressive failure [6,9], tensile cracking [10] and erosion cracking [11], it is almost impossible to perform effective and timely remedial measures, especially for core wall dam projects. Therefore, a scientific understanding of the working behaviour of cut-off walls is very important for ensuring the overall safety of rockfill dam projects in deep overburden areas.

To understand the stress deformation pattern, failure mechanism, and performance characteristics of concrete cut-off walls, numerous scientific research institutions and researchers have performed many studies and achieved beneficial results. Dascal [6] used the observation data of stress and deformation characteristics of the cut-off structure of the Manicouagan 3 dam to comprehensively analyse the mechanical properties of the closed cut-off wall. Brown and Bruggemann [11] conducted a thorough study on the mechanical properties of an enclosed wall caused by the construction design of the Arminou dam. Rice and Duncan [12] collected the operational characteristics of 30 example

* Corresponding author at: The State Key Laboratory of Coastal and Offshore Engineering, Dalian University of Technology, Dalian, Liaoning 116024, China.

E-mail address: quyongqian@dlut.edu.cn (Y. Qu).

<https://doi.org/10.1016/j.engstruct.2024.119497>

Received 11 August 2024; Received in revised form 9 November 2024; Accepted 12 December 2024

Available online 19 December 2024

0141-0296/© 2024 Elsevier Ltd. All rights are reserved, including those for text and data mining, AI training, and similar technologies.

engineering antiseepage structures, and the failure and cracking mechanisms of different structures under various geological conditions were studied. Wen et al. [13,14] collected monitoring and project construction data for 43 examples of cut-off walls in the foundations of rockfill dam projects to study the statistical patterns and controlling mechanisms of different mechanical properties. Rice and Duncan [15], through calculation and analysis of the degree of safety, noted that the most likely cracking location of an antiseepage body is the area between the overburden and the bedrock. He [9] measured the fracture characteristics of plastic concrete and used the dispersion crack model to analyse the fracture failure of the closed cut-off wall of the auxiliary dam of the Cetian Reservoir. Yu et al. [16] used the concrete plastic damage model to study the damage characteristics of the cut-off wall of a core wall rockfill dam foundation and revealed its damage distribution pattern; Sun et al. [17] proposed an effective damage model for a concrete cut-off wall based on peridynamic homogenization, which was applied to the three-dimensional (3D) damage analysis of a closed cut-off wall of a gravel core wall of a rockfill dam.

Most relevant studies have focused on 100-m-deep closed cut-off wall engineering, and few studies on the damage and failure characteristics of the suspended cut-off wall of a rockfill dam on ultra-deep overburden have been conducted. Due to the lack of practical experience for reference in this type of project, numerical simulation has become an important research method. To date, relevant numerical analysis methods face certain difficulties, limiting their further development. The main manifestations are as follows: (1) The stiffness and size differences between the concrete cut-off wall and the overburden layer are large, and the interaction between the two is obvious, which places great requirements on the mesh size. Using a model mesh of a consistent scale, the computational complexity of 3D nonlinear analysis is unbearable. (2) The soil has a strong influence on the cut-off wall, and it is necessary to accurately describe the soil properties. In the numerical simulation of rockfill dams over overburden, the nonlinear elastic model (Duncan–Chang Model) has often been used to describe the soil, but it cannot reflect the real mechanical properties (shear dilatation and cyclic hardening characteristics) of the soil [18]. (3) In the simulation of a cut-off wall, the linear elastic model has frequently been used, and following Yu et al. [16], the plastic damage model has also been gradually used to describe the stiffness and strength degradation characteristics of concrete after damage [19–23]. This model leads to the same reductions in the modulus and strength in the other two directions after damage occurs in one direction. The tensile and compressive damage characteristics interfere with each other, making it difficult to accurately characterize the damage characteristics of concrete under the complex stress state and the induced anisotropy of the material. (4) Existing research typically models concrete cut-off walls within the overburden as continuous concrete structures. However, this modelling approach does not align with the construction techniques of cut-off walls. In reality, concrete cut-off walls are composed of multiple concrete panels. The joints between these panels form structurally weak points, making these locations prone to cracking [11,24–26].

To address the aforementioned issues, this paper aims to establish a multiscale refined analysis model for the stress state of cut-off walls in the ultra-deep overburden of rockfill dams utilizing a coupled finite element method (FEM)-scaled boundary finite element method (SBFEM). The constitutive model for the materials employs the unified generalized plasticity model of elastic–plastic–creep to describe the complex properties of the soil. In addition, a combined concrete plastic damage model and cohesive zone model are used to separately characterize compressive failure and tensile cracking. For the first time, an elastoplastic damage evolution analysis method for the entire system of cut-off walls of rockfill dams on ultra-deep overburden is proposed. Using an asphalt concrete core dam on ultra-deep overburden as a case study, this research analyses the damage and cracking of concrete cut-off walls under complex conditions of construction, impoundment and long-term operation while considering the impact of construction joint

interfaces. The results elucidate the stress deformation patterns of a suspended concrete cut-off wall in ultra-deep overburden, reveal the damage and cracking evolution and failure mechanisms of the concrete cut-off wall, identify weak areas of the cut-off wall, and quantify the degree of damage to the cut-off wall. This study provides theoretical and technical support for the safety evaluation and design optimization of cut-off walls of rockfill dams on ultra-deep overburden.

2. Theoretical method

2.1. Unified generalized plasticity model of elastic–plastic–creep

Compared with the traditional nonlinear elastic model, the elastoplastic model can more reasonably reflect the real mechanical state of the soil body in theory [18,27]. Currently, there are numerous elastoplastic models, including the Pastor–Zienkiewicz constitutive model (generalized plasticity model for short) based on generalized plastic mechanics theory [28] proposed by Pastor et al. [29]. This model has a clear framework, can effectively reflect the deformation characteristics of sand under monotonic and cyclic loading conditions, is easy to program, and has been widely used in finite element numerical analysis in the geotechnical field. However, the original generalized plasticity model has been proposed for sand liquefaction, which is suitable for the scenario in which the change in the confining pressure remains within a small range. This model has certain limitations in static and dynamic numerical analyses of high rockfill dams with large mean principal stress variations. On this basis, the generalized plasticity model can be improved by considering the stress correlation of the dam construction material in terms of the elastic modulus, plastic loading modulus and unloading modulus [30]. The generalized model has been integrated into the GEODYNA software platform and successfully applied to the numerical analysis of rockfill dams, nuclear power plants, underground buildings and other structures [31–34]. To consider the effect of creep (duration) load on sand, Liu et al. [35], based on the improved generalized plasticity model, established a unified generalized plasticity model of elastic–plastic–creep through the description of both the instantaneous strain and creep strain of soil according to the stress–strain–time model, where the creep body strain rate $\dot{\epsilon}_v^t$ and creep shear strain rate $\dot{\epsilon}_s^t$ can be expressed as follows:

$$\dot{\epsilon}_v^t = \alpha_v \epsilon_{vf}^t \left(1 - \frac{\epsilon_{vc}^t}{\epsilon_{vf}^t} \right)^{c_v} \quad (1)$$

$$\dot{\epsilon}_s^t = \alpha_s \epsilon_{sf}^t \left(1 - \frac{\epsilon_{sc}^t}{\epsilon_{sf}^t} \right)^{c_s} \quad (2)$$

$$\epsilon_{vf}^t = c_1 \left(\frac{p'}{p_a} \right)^{m_1} \quad (3)$$

$$\epsilon_{sf}^t = c_2 \left(\frac{p'}{p_a} \right)^{m_2} \eta^{m_3} \quad (4)$$

where ϵ_{vf}^t and ϵ_{sf}^t are the ultimate creep strain and the ultimate creep shear strain, respectively; ϵ_{vc}^t and ϵ_{sc}^t are the cumulative creep strain and the cumulative creep shear strain in period t , respectively; and α_v , α_s , c_v , c_s , c_1 , c_2 , m_1 , m_2 and m_3 are experimentally obtained model constants. For the complete theoretical derivation and the definitions of all parameters, please refer to the literature [35].

2.2. Concrete plastic damage model

As a quasi-brittle material, concrete exhibits linear elastic characteristics under low applied stresses. As the stress increases and the material strength increases, local damage generates microcracks, which exhibit nonlinear stiffness degradation and strain softening

characteristics at the macroscopic level. To reasonably reflect the key characteristics of the abovementioned concrete material, Lubliner et al. [36] proposed the Barcelona plastic damage model based on a combination of plastic theory and the fracture energy-based damage variable, and the yield function of this model is expressed in total stress space. On this basis, Lee and Fenves [37] proposed the plastic damage model, which uses two damage variables—tension and compression—as the description indicators, and an applicable constitutive stress integration method was provided. The yield function of this model is expressed in the effective stress space, which can conveniently describe the plastic damage development of the material and has been widely recognized globally. This model has been widely used in concrete dam [38,39]. Yu et al. [19] integrated the elastoplastic iteration framework and the return map-integration method into the GEODYNA software platform and successfully applied them to the 3D numerical analysis of rockfill dams.

2.3. Cohesive zone model

The cohesive zone model (CZM) theory was first proposed by Dugdale [40] and Barenblatt [41] to describe the processes of crack initiation, propagation, penetration failure, and contact interaction following internal material failure. This model presents fracture behavior as a gradual process, assuming a small cohesive zone at the crack tip where cohesive forces resist the relative separation between interfaces. During cracking, the interface stress is related to the crack displacement and follows a traction-separation law (TSL), which avoids the stress singularities typically encountered at crack tips in linear elastic fracture mechanics [42].

In the application of the CZM for simulating cracking, cohesive interface elements (CIEs) are placed where cracks are expected to initiate and propagate, and these elements are connected to the surrounding solid elements. As loading increases, the stress state in the CIEs reaches the failure criterion, leading to a reduction in stiffness and bearing capacity. When stiffness drops to zero, the CIE fails, resulting in new cracks appearing on the model's surface. Given that the bilinear model is effective for capturing the fracture characteristics of brittle materials and is computationally efficient [43], it is used here to describe the traction-separation relationships within the cohesive elements. This model has been applied to concrete dams [44] but is seldom used in rockfill dam applications. Our research team has previously used the CZM to simulate dynamic cracking in concrete face dams and to assess the effects of seismic measures; for a detailed introduction and validation of this constitutive model, refer to the work by Qu et al. [45].

However, the CZM has two inherent limitations: (1) crack propagation is mesh-dependent, and (2) it does not account for compressive failure. In this study, the CZM is applied to characterize the mechanical properties of the interfaces between vertically oriented construction segments of the seepage cutoff wall. By vertically predefining cohesive elements in line with the actual construction segment locations during mesh division, we effectively address mesh dependency. Furthermore, compressive failure in cutoff walls typically occurs within the material rather than at the interface. The cohesive elements used in this study can transmit compressive stresses and allow for crack opening and closure without losing compressive stiffness during crack closure. Therefore, although the CZM does not simulate compressive failure, this limitation does not impact the validity of the study results.

2.4. Cross-scale refined analysis method

In 1997, Song and Wolf [46] first proposed the fundamental theory of the SBFEM based on the weighted residual method. As a semi-analytical method, it offers high computational accuracy. Moreover, due to its requirement of only boundary discretization, it reduces one computational dimension, making it an effective numerical tool for solving complex polyhedral element problems. This characteristic enables the SBFEM to flexibly handle grid partitioning problems of more

complex geometric shapes, with unparalleled advantages in transitioning between sparse and dense grids in multiscale meshing. Numerous researchers have devoted considerable efforts to the optimization, improvement, and application of this method. Among these, Chen et al. [47] first constructed interpolation functions and displacement-strain matrices for nonlinear analysis based on the original boundary Gauss integration points of the SBFEM. They calculated the relevant coefficient matrices using the material constant stiffness matrix method to avoid the traditional time-consuming and cumbersome computational solving process, thus improving the analysis efficiency. Furthermore, by adding internal Gauss points to solve displacement-strain coordination matrices, element stiffness matrices, and stress integration, they developed polygonal and polyhedral elements suitable for elastoplastic analysis, addressing the limitations of the SBFEM for elastic analysis. Finally, within the same program framework, they integrated the coupled FEM-SBFEM algorithm, developed a multiscale analysis method for the FEM-SBFEM, and applied it to the 3D static-dynamic analysis of rockfill dams [48,49].

3. Analysis model of asphalt core wall rockfill dam on ultra-deep overburden

3.1. Finite element analysis model

In this paper, a high asphalt concrete core wall dam on ultra-deep overburden is considered as an example for analysis. The 3D analysis model is shown in Fig. 1. The dam crest elevation is 1360 m, with a maximum dam height of 140 m. The dam axis is 1840 m, and the width of the river valley at the dam foundation interface is 1480 m. The upstream slope of the dam is 1:2.5, and the downstream slope is 1:2.2. There are upstream and downstream weighting zones, each 250 m long and 40 m high. The overburden is uniformly and horizontally layered, with a total thickness of 530 m, and it is divided into four layers from top to bottom, with thicknesses of 60 m, 20 m, 150 m and 300 m. The joint antiseepage system of an asphalt concrete core wall and a suspended concrete cut-off wall is adopted. The core wall is 138.5 m in height and 2.0 m thick. The thickness at the bottom increases to 2.96 m. The slopes of the left and right banks are 1:1.4 and 1:1.2, respectively. The cut-off wall is 140 m deep, with the bottom extending to the middle of the overburden. The thickness is 1.0 m, and an enlarged end is provided at the connection between the top and the core wall. The two sides of the cut-off wall are embedded 1.0 m deep in the bedrock of the bank slope, with slopes of 1:1 and 1:1.2.

The finite element-scaled boundary finite element-incremental iterative method-preset thin-layer element cross-scale nonlinear analysis method proposed by Zou et al. [50] is used to finely describe the force-bearing state of the concrete cut-off wall. The bottom of the cut-off wall is analysed by using the coupled cross-scale finite element-scaled boundary finite element analysis method. The mesh sizes of the top and bottom of the cut-off wall are both refined from 8 m to 2 m. Thin-layer elements are set at the connected zone of the core wall-cut-off wall and the bottom of the cut-off wall to simulate the large strain-shear deformation characteristics of the local soil in the form of bands. An elaborate and efficient cross-scale analysis model is finally established, with a total of 1.26 million nodes and 1.22 million elements.

3.2. Material parameters

The unified generalized plasticity model is applied to the materials of the dam, the asphalt concrete core wall, and the overburden, with the material parameters presented in Table 1. These parameters were determined based on the results of laboratory triaxial tests. To accurately simulate the interaction characteristics between materials with differing deformation properties, Goodman contact elements [51], suitable for complex conditions, are assembled between the core wall and the transition material, as well as between the cut-off wall and the

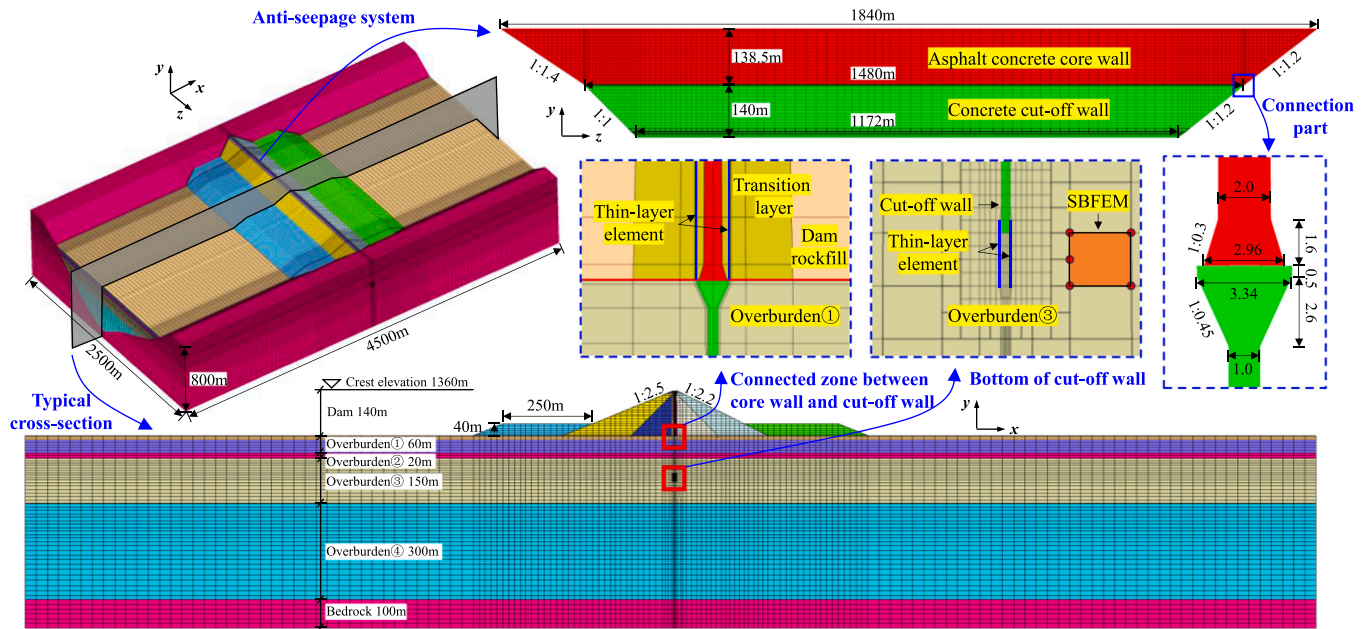


Fig. 1. Finite element analysis model.

Table 1

Parameters for the generalized plasticity model of the dam and overburden material.

Material parameter		Dam			Overburden			
		Rockfill material	Transition material	Asphalt core wall	①	②	③	④
Dry density (g/cm^3)	ρ_d	2.18	2.12	2.392	-	-	-	-
Buoyant density (g/cm^3)	ρ'	-	-	-	1.08	0.99	1.13	1.42
Elastic modulus	G_0	2000	2000	3409	774	350	774	3000
	K_0	1900	1900	169340	844	382	844	2900
	m_s	0.4	0.4	0.193	0.6	0.6	0.6	0.58
	m_v	0.4	0.4	0.193	0.6	0.6	0.6	0.58
Loading direction	M_f	1.5	1.5	1.2	1	1.1	1	1.3
	M_g	1.7	1.7	1.75	1.38	1.4	1.38	1.72
	α_f	0.25	0.25	0.1	0.35	0.15	0.35	0.2
	α_g	0.3	0.2	-0.9	0.6	0.6	0.6	-0.8
Plastic modulus	H_{i0}	1750	2100	440	520	150	480	2000
	m_l	0.2	0.2	0.1	0.35	0.6	0.35	0.55
	β_0	30	30	16	25	25	25	30
	β_1	0.02	0.02	0.04	0.02	0.02	0.02	0.012
	H_{u0}	15000	12600	450	3120	1500	3120	12000
	m_u	0.2	0.2	0.19	0.35	0.6	0.35	0.55
	γ_u	2.5	2.5	10	2.5	3.5	2.5	3
	γ_{DM}	5	5	100	3.5	3	3.5	8
	r_d	2	2	100	2	2	2	5

overburden. The parameters of the generalized plastic interface model are shown in Table 2. C45 concrete is used for the cut-off wall, and the material parameters are shown in Table 3. The bedrock has a linear elastic model with a density of $\rho = 2400 \text{ kg}/\text{m}^3$, an elastic modulus of $E = 13.0 \text{ GPa}$, and a Poisson's ratio of $\nu = 0.25$.

Table 3

Parameters for the concrete plastic damage model.

ρ (g/cm^3)	E (GPa)	ν	f_t (MPa)	f_c (MPa)	G_t (N/m)
2.5	33.5	0.167	2.85	38.5	350

Table 2

Parameters for the generalized plastic interface model.

Location	Elastic modulus		Critical state			Plastic flow direction			Loading direction	Plastic modulus			
	D_{s0} (kPa)	D_{n0} (kPa)	M_c	e_τ	λ	α	r_d	k_m	M_f	k	H_0 (kPa)	f_h	
Asphalt core wall–Transition material	1500	2000	0.88	0.40	0.091	0.65	0.2	0.6	0.65		0.05	8500	2.0
Cutoff wall–Overburden	300	400	0.33	0.61	0.030	0.50	1.0	−0.1	0.25		0.10	1500	2.5

3.3. Dam filling and impoundment

In this study, displacement boundary constraints were applied to define the boundary conditions, with normal constraints on the upstream, downstream, and side banks, and complete constraints at the model base. The self-weight stress field is used as the initial condition for the overburden. The element birth and death method was employed to simulate the staged filling of the dam body, as illustrated in Fig. 2. The dam construction spans 48 months, divided into 106 load increment steps. Upon completion of the dam, the impoundment process begins, with the upstream water level rising to an elevation of 1350 m over a period of 33 months, divided into 70 load increment steps. During impoundment, buoyancy is applied to the submerged portion of the upstream dam body, while hydrostatic pressure is applied to the upstream and downstream surfaces of the seepage control system as surface loads. To ensure stability and accuracy in the calculation results, a high-precision incremental iterative method is employed throughout for implicit solutions. This study used the large-scale geotechnical engineering finite element high-performance analysis software GEO-DYNA7.0 [52], independently developed by Dalian University of Technology. This software integrates the FEM, SBFEM, MFM, and DEM for coupled numerical analysis and is widely applied in both static and dynamic analyses of rockfill dams [3,16,19,30–32,48,50].

4. Results and analysis

4.1. Stress and deformation mode of the cut-off wall

Before discussing the force-bearing and deformation mode of the suspended concrete cut-off wall, it is necessary to understand the overall deformation mode of the dam and the overburden soil. Fig. 3(a) and (b) show the maximum cross-sectional deformation contours of the dam body at the completion of filling and at the completion of impoundment, respectively. At the completion of filling, the basic symmetry of the upstream and downstream dams and the uniformly layered below the dam body, results in overall deformation that is roughly and symmetrically distributed around the dam axis. Additionally, vertical deformation mainly occurs due to the inward sinking of the dam body. The overall maximum vertical settlement is 5.25 m, which occurs at the dam foundation interface. The upstream and downstream cover weights decrease by 0.30 m horizontally. At the completion of impoundment, the overall vertical settlement is minimally affected by the water, with the maximum vertical settlement slightly increasing to 5.30 m. The horizontal hydrostatic pressure acts on the vertical anti-seepage system, causing the relatively large overall deformation to expand in the downstream direction. The increase in deformation in the river direction is shown in Fig. 3(c). Eventually, the maximum downstream

deformation along the river increases to 0.50 m.

The deformation of soil closely affects the load–deformation characteristics of the cut-off wall. Fig. 4 shows the force-bearing condition of the suspended cut-off wall, which is under the joint action of multiple types of loads, such as the upper soil pressure F_s , lateral soil friction F_f , and hydrostatic pressure F_h . Therefore, to facilitate the discussion of the load–deformation characteristics, the linear elastic model is used to describe the cut-off wall in this section.

To characterize the global deformation of the cut-off wall in 3D space, four monitoring feature lines (vertical feature lines L1 and L2 and horizontal feature lines L3 and L4) and a total of four feature points (P1, P2, P3, and P4) are selected, and the locations are shown in Fig. 5. Fig. 6 shows the deformation distribution along the river direction at the corresponding locations of the cut-off wall at different times. At the completion of filling, due to the basic symmetry of the upstream and downstream dams, the overall upstream deformation of the cut-off wall is not large, with a maximum deformation of 8.9 cm at the mid-height of the wall. This location (1140–1160 m elevation) is in the silt clay layer (overburden ②) with a relatively low modulus and high lateral earth pressure. During the water impoundment stage, the hydrostatic pressure leads to downstream deformation of the wall. The increases in the downstream displacements of P1, P2, P3 and P4 are 16.6 cm, 28.1 cm, 20.2 cm and 10.6 cm, respectively. At the completion of impoundment, which is affected by various factors, such as lateral soil pressure, hydrostatic pressure and bedrock constraints, on both sides, the deformation along the river of the cut-off wall eventually exhibits the distribution characteristics of a large river valley, a small area on both sides, a large top and a small bottom. The shoulder (position indicated by point P1) generates downstream bending deformation, causing the downstream side of the wall to bear axial tension.

Fig. 7 shows the vertical deformation distribution at the top of the cut-off wall. At the completion of filling, under the action of dam gravity and overburden friction, the maximum vertical deformation of the cut-off wall is 3.67 m, and it is in the middle of the river valley. Furthermore, obvious reverse bending deformation occurs at the wall shoulders on both sides. At the completion of impoundment, the upstream soil material is affected by buoyancy, which reduces the vertical force on the wall. The cut-off wall rebounds upwards by a small margin of 5.5 cm, and its deformation increment is much smaller than its overall value. In summary, the overall deformation of the suspension-type cut-off wall is dominated by vertical deformation. The bottom of the walls on both sides is supported by the bedrock, and the shoulder section of the top wall exhibits a deformation mode similar to that of an overhanging beam. Fig. 8 shows the deformation profile of the cut-off wall at the completion of impoundment.

Fig. 9 and Fig. 10 show the vertical deformation characteristics of the cut-off wall and the surrounding soil and the distribution of the lateral

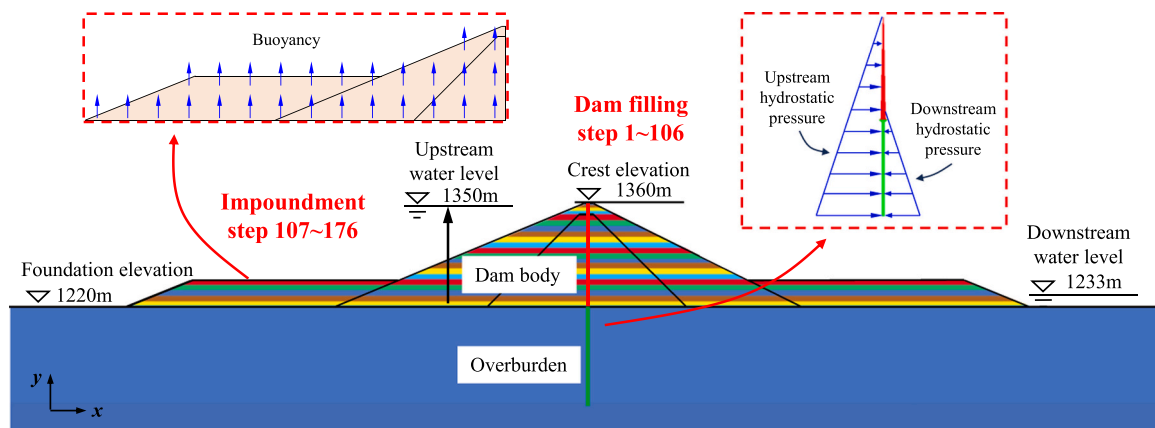


Fig. 2. Schematic diagram of dam filling and impoundment.

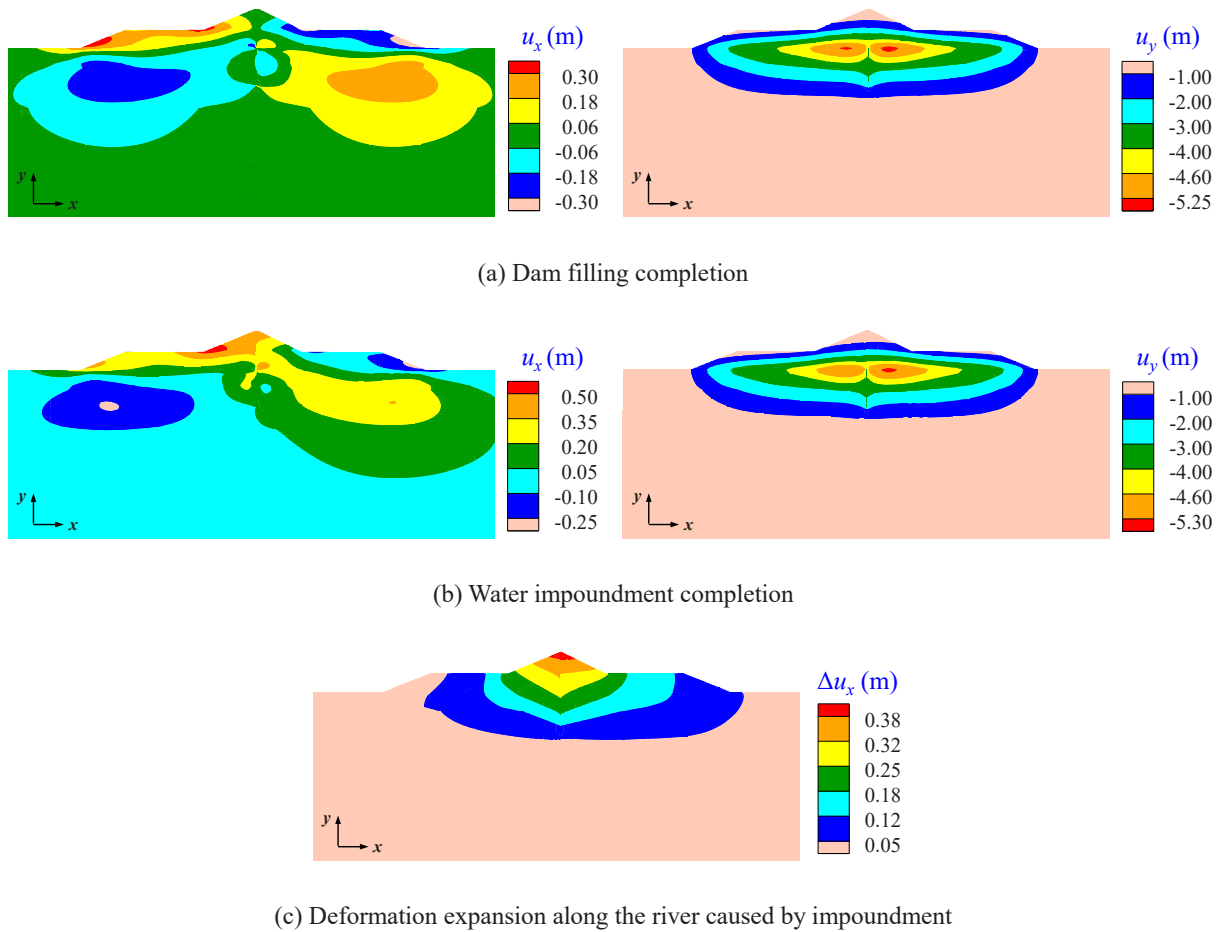


Fig. 3. Maximum cross-sectional deformation diagram of the dam (positive values for downstream deformation and upwards deformation).

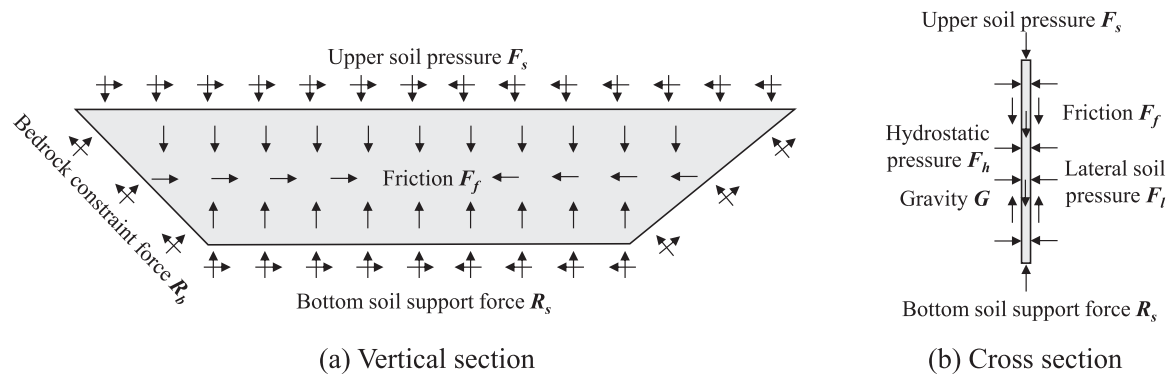


Fig. 4. Schematic diagram of force-bearing on the suspended cut-off wall.

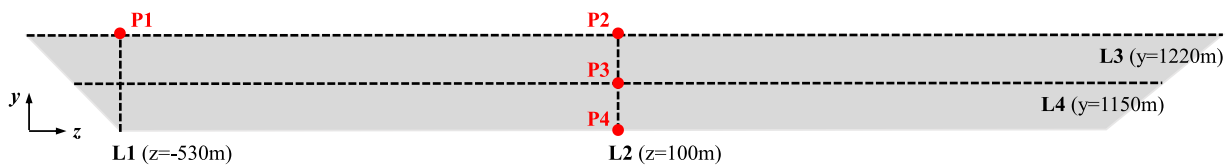


Fig. 5. Schematic diagram of the feature lines for the deformation monitoring of the cut-off wall.

soil friction on the wall at the completion of impoundment, respectively. Under the pressure of the overlying soil and self-weight, the overburden mainly undergoes vertical compressive deformation. Since the modulus of the cut-off wall is much greater than that of the overburden soil, the

wall itself experiences minimal compressive deformation and will penetrate into the soil at both ends. Compared with that of the cut-off wall, the vertical settlement of the overburden layer changes significantly from the top to the bottom, with the upper layer settling more and

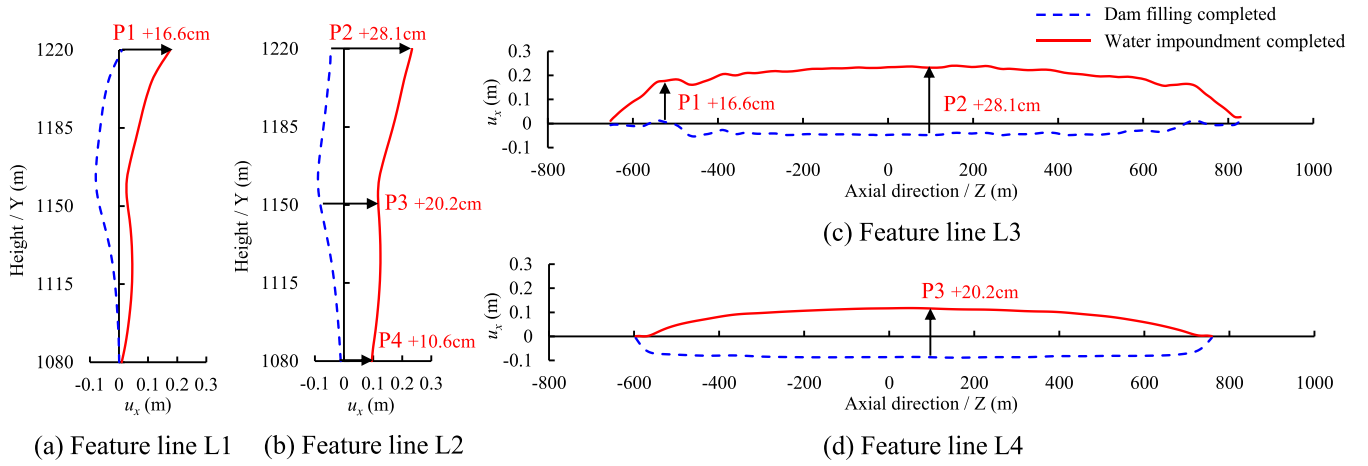


Fig. 6. Deformation distribution of the cut-off wall along the river direction.

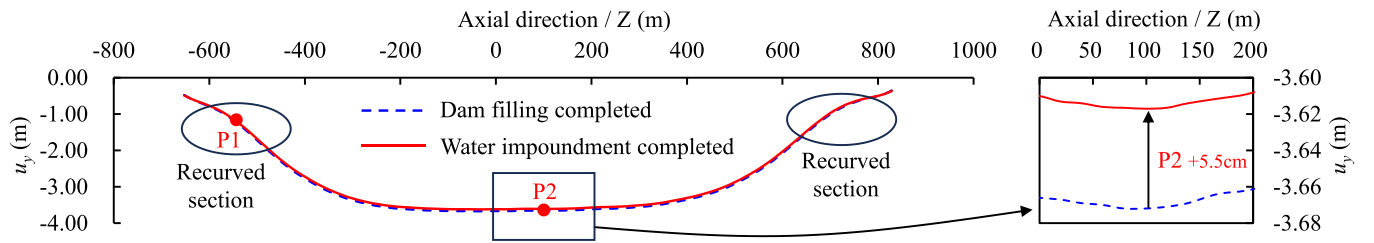


Fig. 7. Vertical deformation distribution at the top of the cut-off wall.

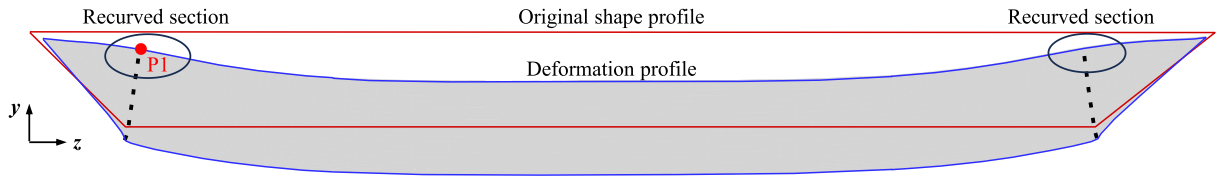


Fig. 8. Deformation profile of the cut-off wall at the completion of impoundment (deformation magnified 20 times).

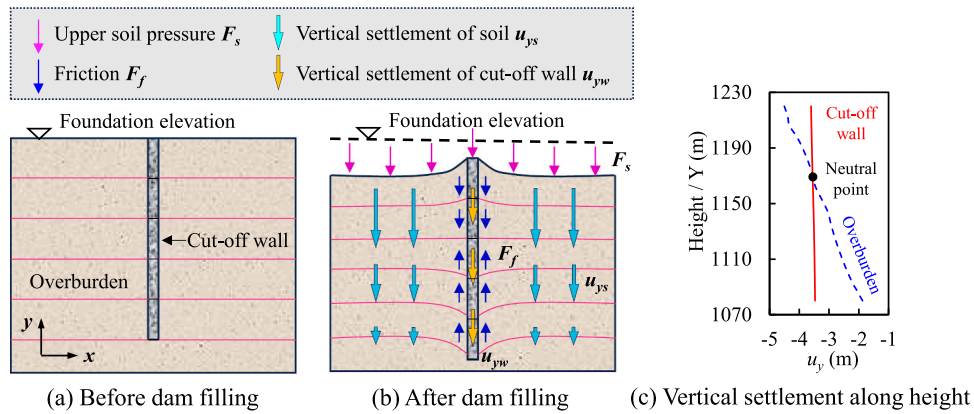


Fig. 9. Vertical settlement diagram of the cut-off wall and the surrounding soil.

the lower layer settling less. Therefore, the upper area of the cut-off wall experiences downwards frictional resistance, the lower area experiences upwards frictional resistance, and a neutral boundary area with zero friction resistance is apparent in the middle.

The stress state distribution of the cut-off wall at the completion of impoundment is shown in Fig. 11. Based on the force-bearing conditions

and deformation modes, the following conclusions can be drawn. (1) The cut-off wall is dominated by vertical deformation. Due to constraints from the bedrock on both sides, the vertical compressive stresses at the bottom on both sides are the largest. The walls in the valley area are subjected to soil friction, and the vertical compressive stress is the largest where the friction direction changes. (2) The support of the cut-

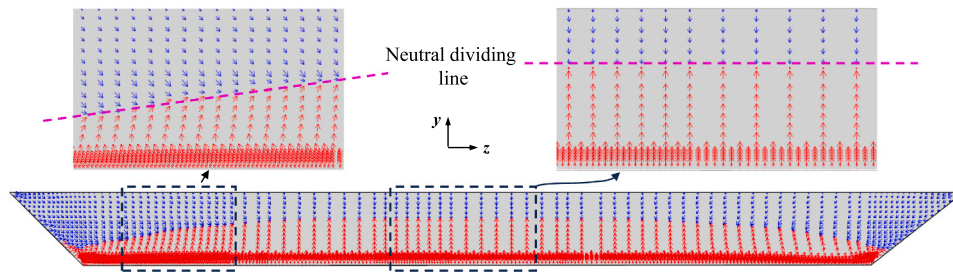


Fig. 10. Direction of the soil friction resistance on the cut-off wall.

off wall by the bedrock on both sides of the bank leads to a deformation mode similar to that of overhanging beams to appear on the left and right sides, and obvious recurved sections appear at the wall shoulders on both sides. Tensile deformation occurs at this position, increasing the axial tensile stress in the dam. After passing through the recurved point, a high compressive stress appears at the top of the cut-off wall, and a high tensile stress occurs at the bottom. The directions of these stresses are both along the dam axis. (3) The shear stress τ_{yz} in the plane (y - z plane) of the cut-off wall is the largest at the bottom on both sides. (4) The maximum compressive stress of the cut-off wall described by the linear elastic model is 180 MPa, and the maximum tensile stress is 40 MPa. The distributions are shown in Fig. 11(d) and (e).

4.2. Failure mechanism of the cut-off wall

As a quasi-brittle material, the nonlinear mechanical properties of concrete cannot be accurately described by traditional linear elastic models. An examination of the stress distribution results of the cut-off wall in the previous section shows that the stress greatly exceeds the concrete strength in the local area of the wall. This incorrect stress state should not be directly used in the safety assessment of cut-off wall structures. In fact, overloading can cause compressive fracture and tensile cracking of the cut-off wall, thus releasing the local high stress. In addition, due to the construction technology of cut-off wall grooves, the vertical distributions of joints in groove sections are unavoidable. The strength and modulus of the joint interface are lower than those of the concrete of the cut-off wall, and cracking is prone to occur at this position (Fig. 12). Therefore, based on the above factors, the concrete plastic damage model and cohesive force model are used in this section to describe the damage and failure characteristics of the cut-off wall. As shown in Fig. 13, vertical CIEs are preset at the joints of the cut-off wall's groove sections to describe the tensile failure characteristics of the wall using a cohesive model. The cut-off wall itself is modelled using solid elements and a plastic damage model to describe its compressive failure characteristics.

Compared to those at the wall, the cohesive zone model parameters at the groove interface are weakened to a certain extent. Due to the lack of test results, the strength reduction factor at the interface between the new and old concrete is referenced in this study [53]. Since the interface of the groove section cannot be processed by dabbing and cleaning, slurry may be present between the walls at the groove interface, which can further reduce the joint surface strength. Therefore, the reduction factor is set to a relatively small value. In the present study, 0.25 is used in the calculations. Notably, the interface of the groove segment of the cut-off wall is arc shaped. To simplify the modelling and calculation processes, the interface of the groove segment is simplified to a plane in the present study.

Linear elastic analysis results of the cut-off wall show that the maximum tensile and compressive stresses are mainly concentrated on the left and right sides of the wall and are basically distributed symmetrically. Therefore, the damage and failure modes at this location require specific attention. Fig. 14 shows the changes in the damage, cracks and stress distribution of the cut-off wall on the left bank. The

details are described as follows:

- (1) The dam is filled to an elevation of 1250 m (step 35). Slight compressive damage occurs at the embedded section at the bottom of the wall and its nearby local area, and the maximum damage factor is 0.2. Vertical cracks appear at the top wall shoulder. The maximum length and width of a single crack are 30 m and 1–2 cm, respectively. Concentrated compressive stress is present at the junction between the bottom of the wall and the bedrock, and the tensile stress is mainly distributed at the wall shoulder.
- (2) With the increase in the dam filling volume, when the dam is filled to an elevation of 1274 m (step 50), the degree of damage at the bottom of the embedded section further increases, and the damage factor increases from 0.2 to 0.8. The concrete is crushed, the stiffness is drastically reduced, the compressive stress is released and transferred upwards, the support point of the bedrock for the cut-off wall is shifted upwards, and the compressive damage of the cut-off wall extends upwards along the embedded section. Furthermore, as the support point of the embedded section on both sides of the cut-off wall moves upwards, the tensile stress area at the bottom of the cut-off wall moves synchronously, and a vertical crack with a width of approximately 2 cm appears at the bottom of the cut-off wall surrounding the support point. The width of the top crack further increases to 3 cm.
- (3) The dam continues to be filled until an elevation of 1304 m is reached (step 75). The scope and extent of the compressive damage of the cut-off wall continue to increase. The cracks at the top and bottom of the cut-off wall further extend, forming a triangular cracking zone. The stress of the wall at the junction of the wall foundation is released, and the tensile stress area moves upwards.
- (4) When dam construction is completed (step 106), more than 90 % of the embedded section of the cut-off wall undergoes compressive damage. The maximum crack width increases to 6 cm and is in the middle of the junction between the wall and the foundation. The stress of the wall at the junction of the wall foundation is released, the tensile stress area shrinks, and the maximum tensile stress is 2.5 MPa.
- (5) After the completion of the filling, the upstream water level is restored to the normal water impoundment level through 70 steps. The hydrostatic pressure minimally impacts the damage, cracks and stress distribution characteristics of the cut-off wall. The area of the area with a final pressure damage factor greater than 0.4 for the cut-off wall on the left bank is approximately 250 m², the area of the region affected by cracking is 5700 m², and the maximum width of a single crack is 6 cm.

After comprehensively analysing the development processes of various indicators of the abovementioned cut-off wall, the damage and cracking evolution diagram is shown in Fig. 15. The cut-off wall is subjected to a vertical load (including gravity G , upper soil pressure F_s ,

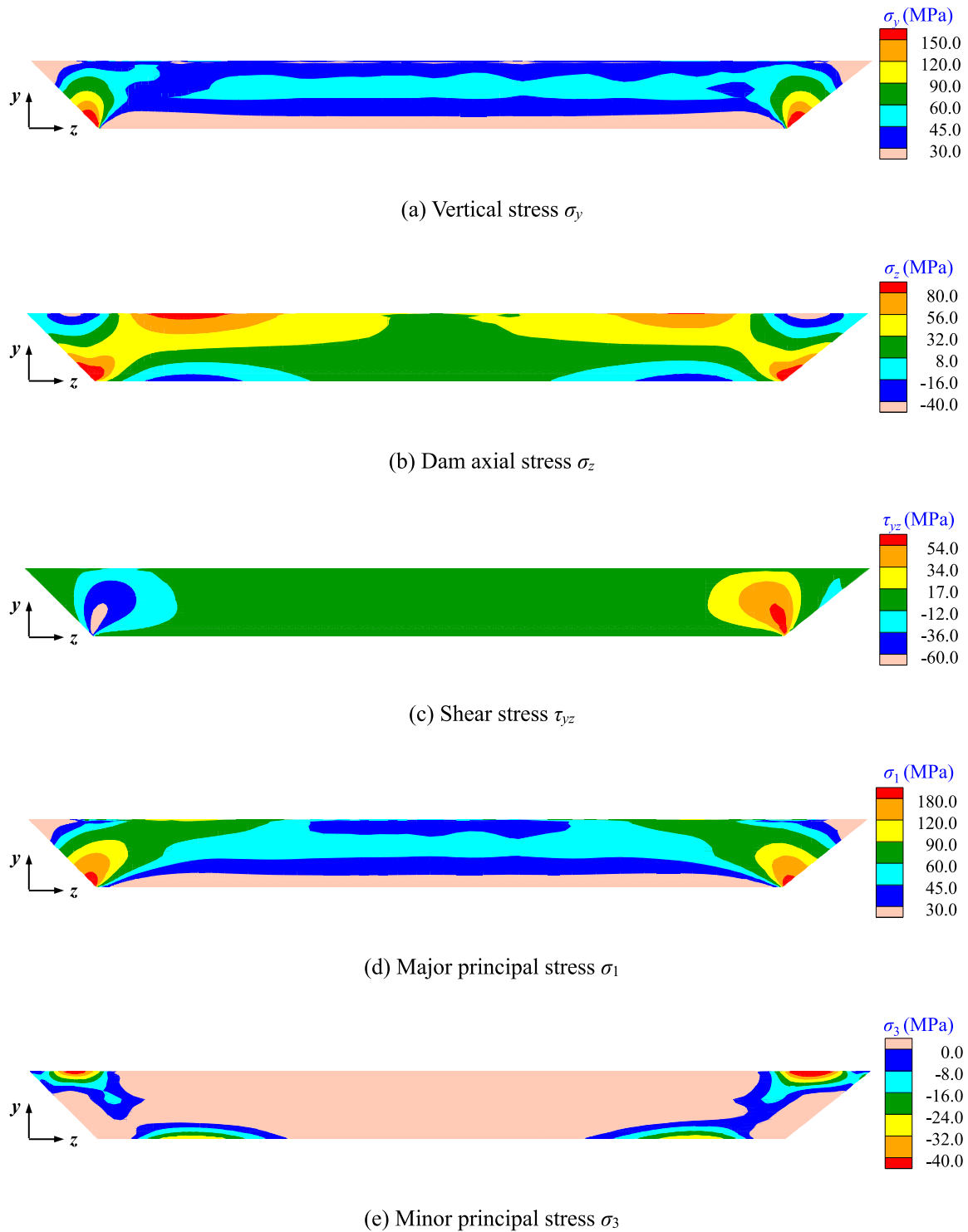


Fig. 11. Stress state of the linear elastic cut-off wall (positive compression and negative tension).

and lateral soil friction F_f) and has bedrock support on both sides. The bottom of the embedded section at the wall foundation junction generates a relatively large compressive stress. When the compressive stress exceeds the compressive strength of the concrete, the wall at this location fractures under compression, the bearing capacity decreases, and the bedrock at the bottom fails to support it. As the main support points move upwards along the embedded section of the wall foundation junction, the axial tensile stress area of the dam at the bottom of the cut-off wall shifts accordingly. The emergence of a large tensile stress causes

cracks in the seams of the groove sections on the weak side of the structure from the bottom to the top. As the dam continues to be filled, the damage range extends upwards along the embedded section, and the scope and width of the cracks both gradually increase. Overall, more than 90 % of the embedded section of the cut-off wall is damaged and fractured, and a triangular cracking zone forms on the left and right sides of the wall.

The overall damage, crack distribution and deformation profiles of the cut-off wall at the completion of impoundment are shown in Fig. 16.

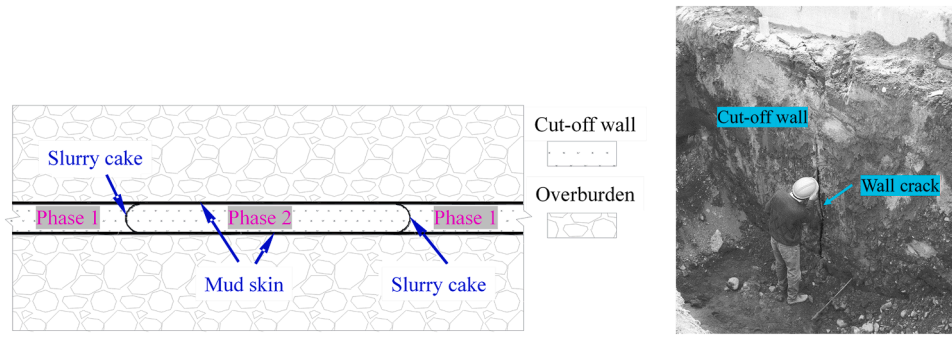


Fig. 12. Cracks in the groove section of the cut-off wall. (a) Schematic diagram of the mud skin surrounding the cut-off wall and the crack in the cut-off wall [26] and (b) crack in the Arminou dam cut-off wall [11].

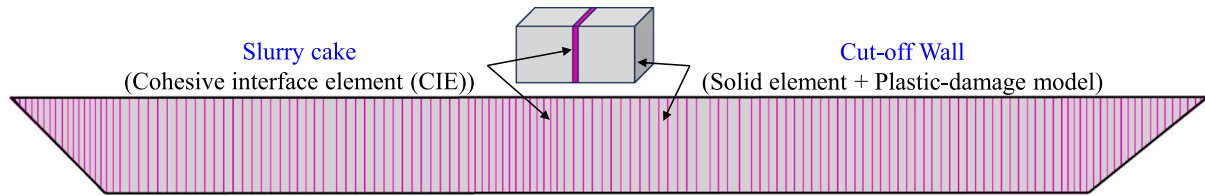


Fig. 13. Schematic diagram of the damage and cracking simulation model of the cut-off wall.

Compressive damage primarily occurs in the embedded sections on the left and right sides of the cut-off wall, with a total area of approximately 550 m² where the damage factor exceeds 0.4, accounting for approximately 0.29 % of the cut-off wall's area. Among these, the maximum damage factor at the bottom of both banks exceeds 0.95. Triangular cracking zones form on both sides of the cut-off wall, with axial lengths of 120 m and 150 m, respectively. The total area affected by cracking is 14000 m², approximately 7.54 % of the cut-off wall's area, and the maximum crack width is 6.0 cm. Compared to elastic analysis, the vertical displacement at the bottom of the cut-off wall's sides is greater when considering damage and cracking, and due to deformation coordination, the reverse bending deformation at the top shoulder of the dam no longer appears. Fig. 17 shows the final stress state distribution of the cut-off wall, indicating significant stress release on both sides of the wall. The top of the cut-off wall in the valley section experiences considerable compressive stress, reaching 41 MPa. This is because the plastic damage model uses multiaxial strength to determine damage, and the cut-off wall in this region is under compression in the axial, vertical, and river flow directions. Therefore, when the maximum compressive stress exceeds the uniaxial compressive strength, the concrete does not necessarily undergo compressive damage. At this time, the maximum tensile stress of the wall is 2.5 MPa, located at the top regions on both sides, primarily composed of shear stress τ_{yz} .

Most material parameters in this study were derived from laboratory experiments, with the exception of the reduction factor for interface strength, which was sourced from the literature [53]. To ensure the reliability and completeness of the simulation results, it is essential to discuss the impact of uncertainties associated with this factor. Fig. 18 shows the distribution of damage and cracking in the cutoff wall when the reduction factor is increased to 0.50. Although this adjustment slightly reduces the extent of damage, it does not alter the overall failure mode or damage pattern within the cutoff wall. Due to the high stress levels encountered by the cutoff wall and the inherent weakness of its segment interfaces in this project, the variability in this parameter is constrained, resulting in a minor effect on the overall results.

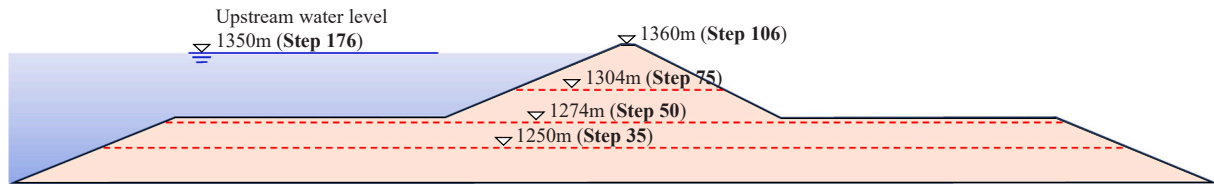
4.3. Effect of creep on cut-off wall

Observations of numerous rockfill dam prototypes [54] and related

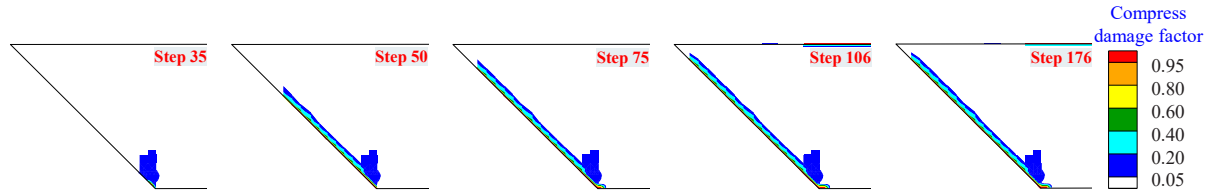
laboratory experimental results [55,56] show that rockfill materials exhibit significant time-dependent creep characteristics, and this characteristic is the main factor causing dam deformation, which often lasts for several years. Excessive late-stage deformation of the dam, especially nonuniform deformation, may damage the seepage control system, posing a potential risk to dam safety [57–60]. Therefore, based on the study in the previous section, the unified generalized plasticity model of Liu et al. [35] with elastic–plastic–creep is used to describe the dam and overburden soil so that its time correlation can be considered to accurately predict the dam deformation attributes and reflect the working characteristics of the cut-off wall. The newly added creep constitutive model parameters for the relevant soils are listed in Table 4. Notably, after the completion of impoundment, the water level upstream of the dam remains constant at an elevation of 1350 m throughout the operational period.

Fig. 19 shows the displacement time history of the characteristic position (dam crest, wall top and wall bottom) of the maximum cross-section of the dam with and without considering creep. A comparison of the two samples shows that because only the instantaneous deformation caused by the incremental load is considered, the deformation of the dam and cut-off wall is generally underestimated by ignoring the creep effect of the soil. After the water impoundment completion period, the plastic hardening of the soil gradually slows the development trend of creep deformation, and the overall deformation generally stabilizes six years after water impoundment completion. Fig. 20 shows the maximum cross-sectional deformation of the dam and thus its stability. The maximum deformation along the river is 0.24 m (upstream) and 1.00 m (downstream), and the maximum vertical settlement increases to 6.40 m, which is an increase of approximately 20 % from that without considering creep.

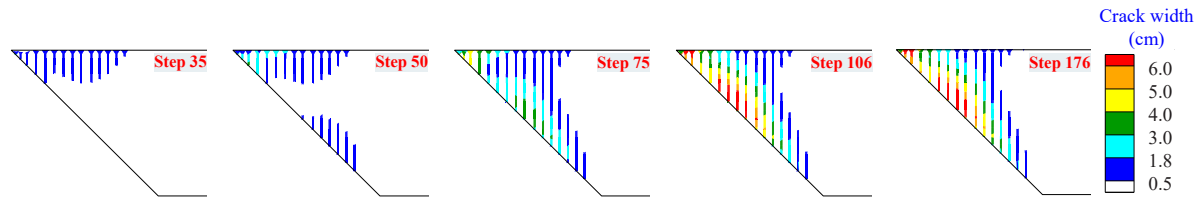
Fig. 21 shows the distribution of damage and cracks on the cut-off wall in the stable period. A comparison with Fig. 16(a) and (b) shows that, due to creep, the overall damage cracking distribution pattern of the cut-off wall has little effect, which is mainly reflected in the increase in magnitude. Specifically, compressive damage occurs on both the left and right sides of the cut-off wall, with the areas of moderate to severe damage (damage factor exceeding 0.4) totalling approximately 560 m². Cracks with ranges of 130 m × 133 m and 160 m × 132 m are generated on the left and right sides of the cut-off wall, respectively. In addition, a



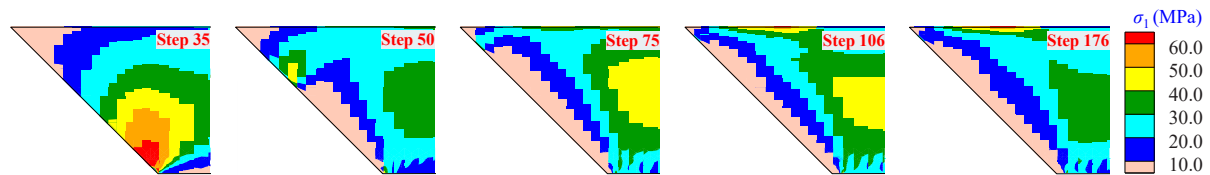
(a) Schematic diagram of the filling elevation and its corresponding calculation steps



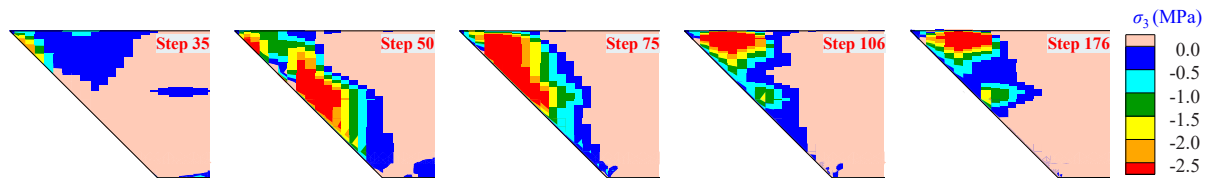
(b) Compression damage distribution and evolution



(c) Crack development



(d) Distribution and evolution of the major principal stress



(e) Distribution and evolution of the minor principal stress

Fig. 14. Changes in the damage, cracks and stress distribution characteristics of the cut-off wall on the left bank.

narrow crack area with a width of 175 m appears at the bottom on the right side. The total area affected by cracking reaches 17000 m², which is an increase of approximately 21 % from that without considering creep. The maximum crack width reaches 8.0 cm, which is an increase of 33 %, and it is in the middle of the junction of the wall foundations on both sides.

5. Conclusions

This study has proposed a novel elastoplastic failure refinement analysis method to address the issues of challenging analysis of the cut-

off wall of rockfill dams on ultra-deep overburden under complex conditions of construction, impoundment, and long-term operations. A unified elastic-plastic-creep model was applied to investigate the mechanical properties of the dam and overburden. Plastic damage model and cohesive zone model were combined to describe the compressive damage and tensile cracking of concrete cut-off walls, respectively. Based on a real-life rockfill dam project, the damage and cracking evolution of the suspended concrete cut-off wall were investigated considering the construction joints. The impact of rockfill and overburden creep on the cut-off wall was discussed. The main findings of the study are concluded as follows:

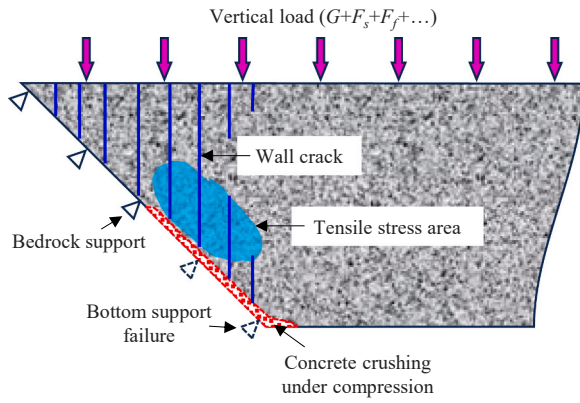
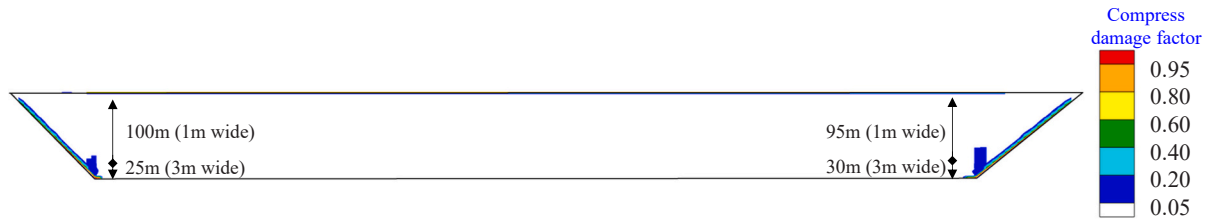


Fig. 15. Schematic diagram of the damage and cracking evolution of the cut-off wall.

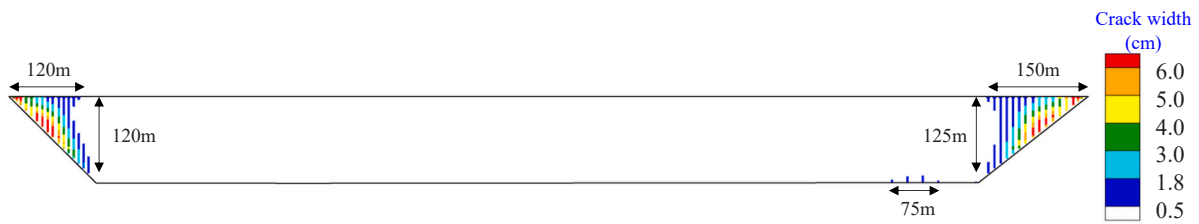
- (1) This paper presents an advanced method for the cut-off walls of the rockfill dam on ultra-deep overburden. The proposed method can describe the damage and cracking evolutions, reflect the stress redistribution characteristics of damaged concrete, precisely locate weak areas, quantify the degree of damage, and reveal the real engineering behaviour of cut-off walls.
- (2) Under construction and impoundment conditions, the overall deformation of the suspension cut-off wall is mainly vertical. The bedrock support on both sides of the wall generates a high stress perpendicular to the bank slope at the bottom of the wall on both

sides. Furthermore, the in-plane bending deformations of the overhanging beams at the top of the two sides lead to high axial tensile stress in the dam wall shoulder. As the deformation extends towards the valley, after passing the inflection point, a high axial compressive stress appears at the top of the cut-off wall, and a high axial tensile stress appears at the bottom of the cut-off wall.

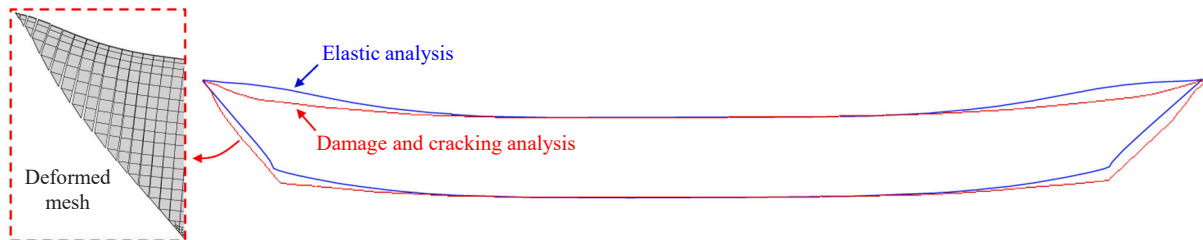
- (3) The compressive deformation of the overburden under the weight of the dam is significant. The top and bottom of the cut-off wall penetrate the soil. The cut-off wall in the central part of the valley is subjected to mainly the vertical friction resistance from the overburden. The upper region is subjected to downwards friction resistance, and the lower region bears upwards frictional resistance. Therefore, the maximum vertical compressive stress of the cut-off wall appears at the neutral boundary, where the direction of friction changes.
- (4) The high compressive stress acting perpendicular to the bank slope induces compressive damage at the bottom of the cut-off wall, progressing upwards along the wall–foundation junction as the dam fills. This damage reduces the stiffness and bearing capacity of the affected area, causing the support position of the cut-off wall to shift upwards. Concurrently, the axial tensile stress region at the bottom of the cut-off wall shifts, resulting in vertical cracks that propagate from the bottom to the top at the construction joint and connect with cracks extending downward from the top. These interactions lead to the formation of triangular cracking zones on both sides of the cut-off wall. When considering the creep effects of rockfill and overburden, the location of damage in the cut-off wall remains largely unchanged;



(a) Compression damage distribution



(b) Crack distribution (unit: cm)



(c) Comparison of the deformation profiles (deformation magnification 20 times)

Fig. 16. Damage, crack distribution and deformation profiles of the cut-off wall.

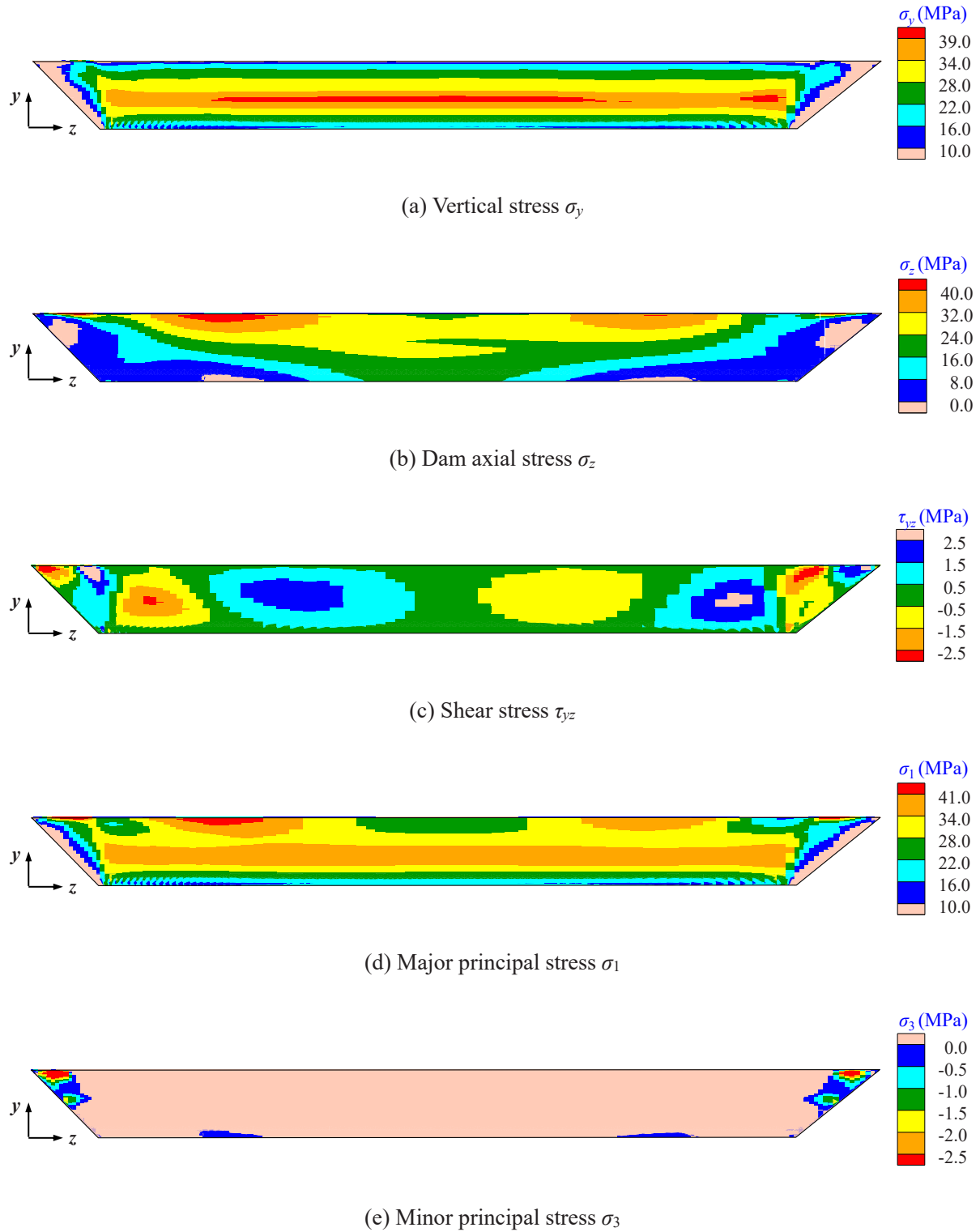


Fig. 17. Stress state of the cut-off wall considering damage and cracking (positive compression and negative tension).

however, the extent of cracking increases by 21 %, and the maximum crack width expands by 33 %.

The proposed method can quantify the degree of damage of the cut-off wall and establish a direct relationship with its anti-seepage performance, which lays the foundation for subsequent seepage analysis and functional assessment. This paper provides theoretical and technical support for the safety evaluation and design optimisation of the cut-off

wall of rockfill dams on ultra-deep overburden.

Author statement

I confirm that all authors have agreed to the submission of this manuscript to Engineering Structures and are aware of its submission.

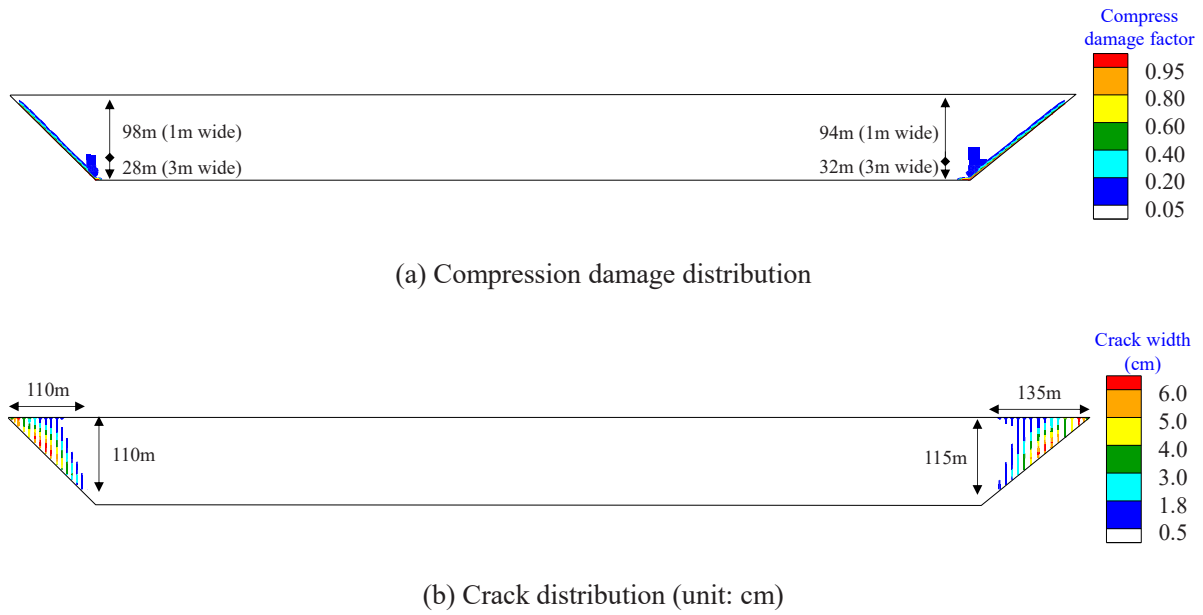


Fig. 18. Distribution of damage and cracking in the cut-off wall (reduction factor 0.50).

Table 4
Parameters for the creep constitutive model of the dam and overburden.

Material partition		α_v	α_s	c_v	c_s	c_1	c_2	m_1	m_2	m_3
Dam		3.5×10^{-3}	3.5×10^{-3}	1.0	1.0	2.7×10^{-4}	1.11×10^{-2}	0.9	0	2.5
Overburden	①	1.0×10^{-3}	1.0×10^{-3}	1.0	1.0	2.7×10^{-4}	8.61×10^{-3}	0.9	0	2.5
	②	5.0×10^{-4}	5.0×10^{-4}	1.0	1.0	4.5×10^{-4}	8.61×10^{-3}	0.9	0	2.5
	③ and ④	1.0×10^{-3}	1.0×10^{-3}	1.0	1.0	2.7×10^{-4}	9.84×10^{-3}	0.9	0	2.5

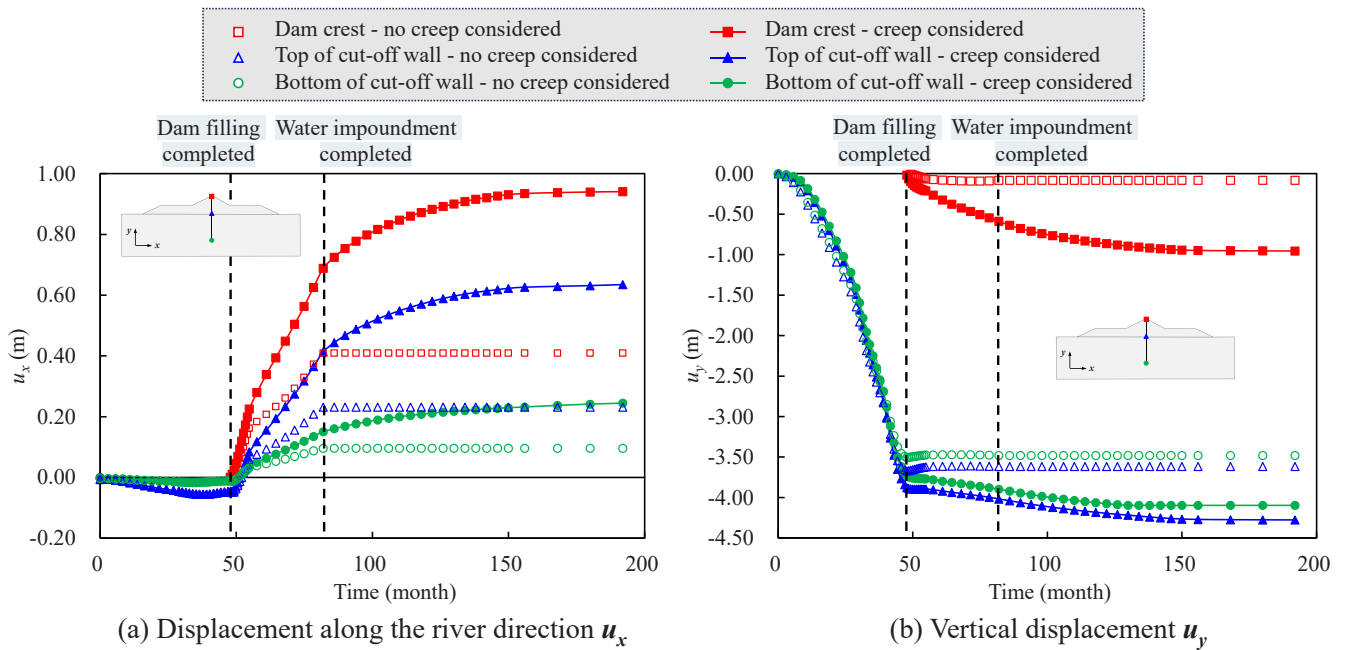


Fig. 19. Displacement time history of feature points on the maximum cross-section of the dam.

CRedit authorship contribution statement

Jun Peng: Writing – review & editing, Writing – original draft, Validation, Formal analysis. **Yongqian Qu:** Writing – review & editing, Supervision, Methodology. **Degao Zou:** Writing – review & editing,

Software. **Jingmao Liu:** Methodology. **Kai Chen:** Methodology.

Declaration of Competing Interest

The authors declare that they have no known competing financial

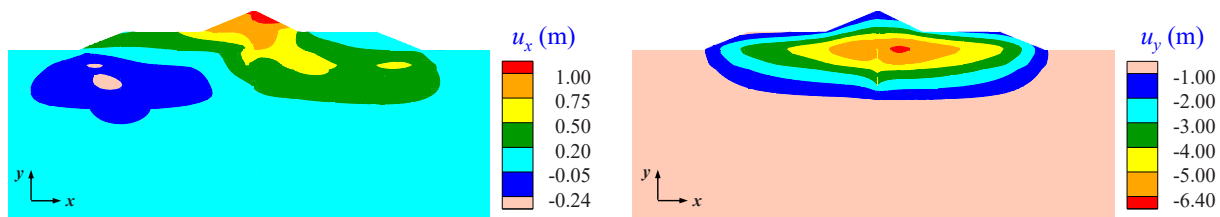


Fig. 20. Deformation diagram of the maximum cross-section of the dam in the stable period (the downstream and upwards deformations are positive).

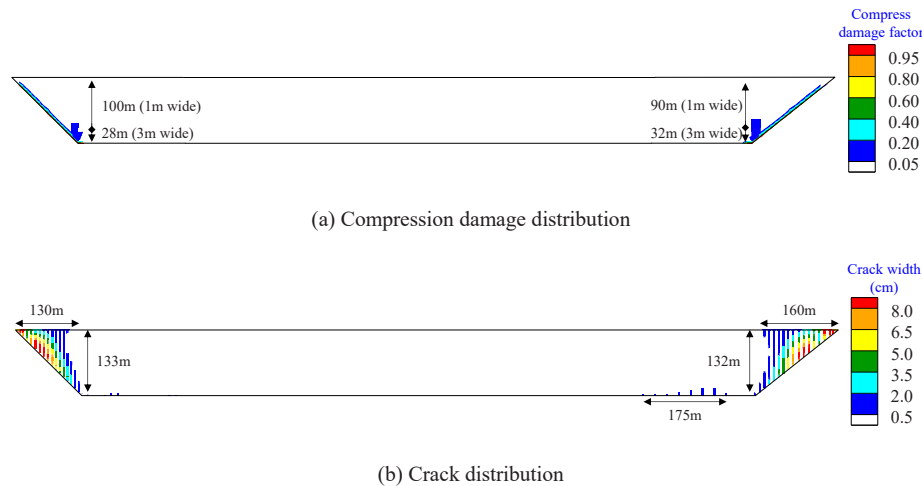


Fig. 21. Distribution of damage and cracks on the cut-off wall in the stable period.

interests or personal relationships that could have appeared to influence the work reported in this paper.

Acknowledgements

This work was supported by the National Natural Science Foundation of China (Grant Nos. 52192674, 52109151, U23B20149, 5240090382).

Data Availability

Data will be made available on request.

References

- [1] Chen H, Ren G, Nie D, Wan Z, Yang T. Engineering geological characteristics of deep overburden in river valleys and its evaluation (in Chinese). *Geol Hazards Environ Prot* 1996;54–60.
- [2] Chen S. Research progresses in key technologies for construction and longterm safety protection of extra high earth-rock dams under complicated conditions. *Sci Sin Technol* 2018;48:1040–8.
- [3] Yu X, Lai Y, Qu Y, Wang Y, Li M. Study on seismic wave propagation regularity and dam-foundation interaction characteristics of earth-rock dam on deep overburden. *Comput Geotech* 2023;164. <https://doi.org/10.1016/j.compgeo.2023.105803>.
- [4] Nenghui Li, Zhankuan MI, Dawei SUN. Study on affecting factors of stress-deformation of diaphragm walls for concrete face rockfill dams built on thick alluvium deposit. *Chin J Geotech Eng* 2007;29:26–31.
- [5] Dang L, Fang G. Practice and development of dam construction using the overburden (in Chinese). *Symposium on Dam Construction Technology Using Deep Overburden* by the Professional Committee of Hydraulic Engineering and Hydroelectric Power Station Buildings of China Hydropower Engineering Society. 2009.
- [6] Dascal O. Structural behaviour of the Manicouagan 3 cutoff. *Can Geotech J* 1979; 16:200–21. <https://doi.org/10.1139/t79-017>.
- [7] Wang W, Hoeg K, Zhang Y. Design and performance of the Yele asphalt-core rockfill dam. *Can Geotech J* 2010;47:1365–81. <https://doi.org/10.1139/t10-028>.
- [8] Xiong K, He Y, Wu X, Dong Y. Stress and deformation behavior of foundation gallery of Changheba Hydropower Station. *Chin J Geotech Eng* 2011;33:1767–74.
- [9] He S. *Fracture Test Of Plastic Concrete And Research On The Fracture Damage Of Seepage Control Wall*. Beijing: Tsinghua University; 1993.
- [10] Ma X, Chen S. Analysis of cracks in asphalt concrete panels of Niutoushan Reservoir dam and measures for removing and reinforcing them (in Chinese). *J Zhejiang Water Conserv Hydropower Coll* 2008;17–20.
- [11] Brown AJ, Bruggemann DA. Arminou Dam, Cyprus, and construction joints in diaphragm cut-off walls. *Geotechnique* 2002;52:3–13. <https://doi.org/10.1680/geot.2002.52.1.3>.
- [12] Rice JD, Duncan JM. Findings of case histories on the long-term performance of seepage barriers in dams. *J Geotech Geoenviron Eng* 2010;136:2–15. [https://doi.org/10.1061/\(asce\)gt.1943-5606.0000175](https://doi.org/10.1061/(asce)gt.1943-5606.0000175).
- [13] Wen L, Chai J, Xu Z, Qin Y, Li Y. A statistical analysis on concrete cut-off wall behaviour. *Proc Inst Civ Eng-Geotech Eng* 2018;171:160–73. <https://doi.org/10.1680/jgeen.17.00142>.
- [14] Wen L, Li Y, Chai J. Statistical analysis of mechanical properties of dam foundation concrete cutoff wall. *J Hydraul Eng* 2021;52:241–54. <https://doi.org/10.13243/j.cnki.slxb.20200315>.
- [15] Rice JD, Duncan JM. Deformation and CRacking of Seepage Barriers in Dams due to CHanges in the Pore Pressure Regime. *J Geotech Geoenviron Eng* 2010;136: 16–25. [https://doi.org/10.1061/\(asce\)gt.1943-5606.0000241](https://doi.org/10.1061/(asce)gt.1943-5606.0000241).
- [16] Yu X, Kong X, Zou D, Zhou Y, Hu Z. Linear elastic and plastic-damage analyses of a concrete cut-off wall constructed in deep overburden. *Comput Geotech* 2015;69: 462–73. <https://doi.org/10.1016/j.compgeo.2015.05.015>.
- [17] Sun W, Bao S, Zhang G. An equivalent damage model of concrete cut-off wall based on homogenization of peridynamics. *J Tongji Univ Nat Sci* 2022;50:1240–50. <https://doi.org/10.11908/j.issn.0253-374x.222323>.
- [18] Liu J. *Elasto-plastic constitutive models of rockfill material and soil-structure interface and their applications on concrete-faced rockfill dam* [PhD. Dalian: Dalian University of Technology; 2015].
- [19] Yu X, Kong X, Zou D, Zhou Y. 3D valley effect mechanism and damage behavior of the concrete cut-off wall in overburden. *J Hydraul Eng* 2019;50:1123–34. <https://doi.org/10.13243/j.cnki.slxb.20190385>.
- [20] Wen L, Li Y, Chai J. Plastic-damage analysis of concrete cutoff wall for a concrete face rockfill dam. *Proc Inst Civ Eng-Geotech Eng* 2020;173:153–68. <https://doi.org/10.1680/jgeen.19.00006>.
- [21] Wen L, Li Y, Chai J. Numerical analysis of plastic damage of concrete cutoff wall for concrete face rockfill dam. *J Hydraul Eng* 2021;52:673–88. <https://doi.org/10.13243/j.cnki.slxb.20200721>.
- [22] Guan Z, Sun X, Zhang G, Li G, Huang P, Zhang B, et al. Deformation and damage behavior of the deep concrete cut-off wall in core earth-rock dam foundation based on plastic damage model - a case study. *Structures* 2022;46:1480–94. <https://doi.org/10.1016/j.istruc.2022.10.136>.
- [23] Bu P, Li Y, Li Y, Wen L, Wang J, Zhang X. Creep damage coupling model of concrete based on the statistical damage theory. *J Build Eng* 2023;63. <https://doi.org/10.1016/j.jobbe.2022.105437>.
- [24] Li Q, Cheng Z. Analysis of the behaviour of stage II cofferdam of TGP. *Chin J Geotech Eng* 2005;27:410–3.

- [25] Soroush A, Soroush M. Parameters affecting the thickness of bentonite cake in cutoff wall construction: case study and physical modeling. *Can Geotech J* 2005; 42:646–54. <https://doi.org/10.1139/t04-090>.
- [26] Yu X. Study on methods for the static and dynamic analysis of earth dam constructed on deep overburden [PhD]. Dalian: Dalian University of Technology; 2017.
- [27] Dong W, Hu L, Yu YZ, Lv H. Comparison between Duncan and Chang's EB Model and the generalized plasticity model in the analysis of a high earth-rockfill dam. *J Appl Math* 2013. <https://doi.org/10.1155/2013/709430>.
- [28] Zienkiewicz OC, Mroz Z. Generalized plasticity formulation and applications to geomechanics. *Mech Eng Mater* 1984;44:655–80.
- [29] Pastor M, Zienkiewicz OC, Chan AHC. Generalized plasticity and the modelling of soil behaviour. *Int J Numer Anal Methods Geomech* 1990;14:151–90. <https://doi.org/10.1002/nag.1610140302>.
- [30] Zou D, Xu B, Kong X, Liu J, Zhou Y. Static and dynamic analysis of high concrete-faced rockfill dam based on generalized plastic model. *J Hydroelectr Eng* 2011;30: 109–16.
- [31] Xu B, Zou D, Liu H. Three-dimensional simulation of the construction process of the Zipingpu concrete face rockfill dam based on a generalized plasticity model. *Comput Geotech* 2012;43:143–54. <https://doi.org/10.1016/j.compgeo.2012.03.002>.
- [32] Zou D, Xu B, Kong X, Liu H, Zhou Y. Numerical simulation of the seismic response of the Zipingpu concrete face rockfill dam during the Wenchuan earthquake based on a generalized plasticity model. *Comput Geotech* 2013;49:111–22. <https://doi.org/10.1016/j.compgeo.2012.10.010>.
- [33] Zou D, Sui Y, Chen K. Plastic damage analysis of pile foundation of nuclear power plants under beyond-design basis earthquake excitation. *Soil Dyn Earthq Eng* 2020; 136. <https://doi.org/10.1016/j.soildyn.2020.106179>.
- [34] Pang R, Chen K, Fan Q, Xu B. Stochastic ground motion simulation and seismic damage performance assessment of a 3-D subway station structure based on stochastic dynamic and probabilistic analysis. *Tunn Undergr Space Technol* 2022; 126. <https://doi.org/10.1016/j.tust.2022.104568>.
- [35] Liu J, Zou D, Ning F, Kong X. A unified constitutive model for instantaneous elastic-plastic and time-dependent creep behaviour of gravelly soils under complex loading. *Can Geotech J* 2023;60:1613–28. <https://doi.org/10.1139/cgj-2022-0635>.
- [36] Lubliner J, Oliver J, Oller S, Onate E. A plastic-damage model for concrete. *Int J Solids Struct* 1989;25:299–326. [https://doi.org/10.1016/0020-7683\(89\)90050-4](https://doi.org/10.1016/0020-7683(89)90050-4).
- [37] Lee JH, Fenves GL. Plastic-damage model for cyclic loading of concrete structures. *J Eng Mech-Asce* 1998;124:892–900. [https://doi.org/10.1061/\(asce\)0733-9399\(1998\)124:8\(892\)](https://doi.org/10.1061/(asce)0733-9399(1998)124:8(892)).
- [38] Lee J, Fenves GL. A plastic-damage concrete model for earthquake analysis of dams. *Earthq Eng Struct Dyn* 1998;27:937–56. [https://doi.org/10.1002/\(sici\)1096-9845\(199809\)27:9<937::Aid-eqe764>3.0.Co;2-5](https://doi.org/10.1002/(sici)1096-9845(199809)27:9<937::Aid-eqe764>3.0.Co;2-5).
- [39] Pan J, Zhang C, Wang J, Xu Y. Seismic damage-cracking analysis of arch dams using different earthquake input mechanisms. *Sci China Ser E-Technol Sci* 2009;52: 518–29. <https://doi.org/10.1007/s11431-008-0303-6>.
- [40] Dugdale DS. Yielding of steel sheets containing slits. *J Mech Phys Solids* 1960;8: 100–4. [https://doi.org/10.1016/0022-5096\(60\)90013-2](https://doi.org/10.1016/0022-5096(60)90013-2).
- [41] Barenblatt GI. The mathematical theory of equilibrium cracks in brittle fracture. *Adv Appl Mech* 1962;7:55–129. [https://doi.org/10.1016/S0065-2156\(08\)70121-2](https://doi.org/10.1016/S0065-2156(08)70121-2).
- [42] Dai Q, Ng K. 2D cohesive zone modeling of crack development in cementitious digital samples with microstructure characterization. *Constr Build Mater* 2014;54: 584–95. <https://doi.org/10.1016/j.conbuildmat.2013.12.095>.
- [43] Alfano G. On the influence of the shape of the interface law on the application of cohesive-zone models. *Compos Sci Technol* 2006;66:723–30. <https://doi.org/10.1016/j.compscitech.2004.12.024>.
- [44] Pan J, Zhang C, Xu Y, Jin F. A comparative study of the different procedures for seismic cracking analysis of concrete dams. *Soil Dyn Earthq Eng* 2011;31: 1594–606. <https://doi.org/10.1016/j.soildyn.2011.06.011>.
- [45] Qu Y, Zou D, Kong X, Yu X, Chen K. Seismic cracking evolution for anti-seepage face slabs in concrete faced rockfill dams based on cohesive zone model in explicit SBFEM-FEM frame. *Soil Dyn Earthq Eng* 2020;133. <https://doi.org/10.1016/j.soildyn.2020.106106>.
- [46] Song C, Wolf JP. The scaled boundary finite-element method - Alias consistent infinitesimal finite-element cell method - for elastodynamics. *Comput Methods Appl Mech Eng* 1997;147:329–55. [https://doi.org/10.1016/s0045-7825\(97\)00021-2](https://doi.org/10.1016/s0045-7825(97)00021-2).
- [47] Chen K, Zou D, Kong X, Chan A, Hu Z. A novel nonlinear solution for the polygon scaled boundary finite element method and its application to geotechnical structures. *Comput Geotech* 2017;82:201–10. <https://doi.org/10.1016/j.compgeo.2016.09.013>.
- [48] Chen K, Zou D, Kong X, Yu X. An efficient nonlinear octree SBFEM and its application to complicated geotechnical structures. *Comput Geotech* 2018;96: 226–45. <https://doi.org/10.1016/j.compgeo.2017.10.021>.
- [49] Chen K, Zou D, Kong X, Liu J. Elasto-plastic fine-scale damage failure analysis of metro structures based on coupled SBFEM-FEM. *Comput Geotech* 2019;108: 280–94. <https://doi.org/10.1016/j.compgeo.2018.12.030>.
- [50] Zou D, Qu Y, Kong X, Chen K, Liu J, Gong J. Refined analysis on stress state of cutoff wall of high asphaltic core dam on super-deep overburden. *Rock Soil Mech* 2023;44:1826–36. <https://doi.org/10.16285/j.rsm.2022.5985>.
- [51] Goodman RE, Taylor RL, Brekke TL. A model for the mechanics of jointed rock. *J Soil Mech Found Div* 1968;94:637–59. <https://doi.org/10.1061/JSEFAQ.0001133>.
- [52] Zou D, Kong X, Liu J, Chen K, Qu Y. Theoretical Introduction and User Manual of the GEODYNA 7.0: A High-Performance Finite Element Analysis Software System for Large-Scale Geotechnical Engineering. Dalian: Dalian: Institute of Earthquake Engineering, Dalian University of Technology; 2022.
- [53] Yang C. Strength of the interface between old and new concrete bond and its process technology (in chinese). *Mar Eng* 1995;49–54. <https://doi.org/10.16233/j.cnki.issn1002-4972.1995.06.013>.
- [54] Dascal O. Postconstruction deformations of Rockfill Dams. *J Geotech Eng-Asce* 1987;113:46–59. [https://doi.org/10.1061/\(ASCE\)0733-9410\(1987\)113:1\(46\)](https://doi.org/10.1061/(ASCE)0733-9410(1987)113:1(46)).
- [55] Cheng Z, Ding H. Creep test for rockfill. *Chin J Geotech Eng* 2004;26:473–6.
- [56] Oldecop LA, Alonso EE. Theoretical investigation of the time-dependent behaviour of rockfill. *Geotechnique* 2007;57:289–301. <https://doi.org/10.1680/geot.2007.57.3.289>.
- [57] Zhang BY, Wang JG, Shi RF. Time-dependent deformation in high concrete-faced rockfill dam and separation between concrete face slab and cushion layer. *Comput Geotech* 2004;31:559–73. <https://doi.org/10.1016/j.compgeo.2004.07.004>.
- [58] Zhang B, Chen T, Peng C, Qian X, Jie Y. Experimental study on loading-creep coupling effect in rockfill material. *Int J Geomech* 2017;17. [https://doi.org/10.1061/\(ASCE\)GM.1943-5622.0000938](https://doi.org/10.1061/(ASCE)GM.1943-5622.0000938).
- [59] Wen L, Cao W, Li Y. Behavior of a concrete-face rockfill dam cutoff wall considering the foundation seepage-creep coupling effect. *Int J Geomech* 2023;23. <https://doi.org/10.1061/jignai.Gmeng-8177>.
- [60] Wen L, Wu L, Li Y. Seepage-creep coupling analysis of concrete-face rockfill dam built on alluvium foundation. *Int J Geomech* 2023;23. <https://doi.org/10.1061/jignai.Gmeng-8946>.